Available online at www.sciencedirect.com
ScienceDirect
Solar Energy 83 (2009) 2205–2216
SOLAR ENERGY
www.elsevier.com/locate/solener

A proposed design and fabrication of lenses and mirrors from a set of spherical rings that produce desired energy distributions for solar energy applications

Jorge González-García [a,c,*], Sergio Vazquez-Montiel [b], Agustin Santiago-Alvarado [a,b], Alberto Cordero-Dávila [c], Graciela Castro-González [a]

[a] Universidad Tecnológica de la Mixteca UTM, Km 2.5 Carretera a Acatlima, Huajuapan de León Oaxaca, C. P. 69000, Mexico
[b] Instituto de Óptica, Instituto Nacional de Astrofísica, Óptica y Electrónica INAOE, Santa María, Tonantzintla Puebla, Apartado Postal 51 y 216, Mexico
[c] Facultad de Ciencias Físico-Matemáticas, Benemérita Universidad Autónoma de Puebla BUAP, Apartado Postal 1152, 72570 Puebla, Mexico

Received 8 August 2008; received in revised form 11 August 2009; accepted 3 September 2009
Available online 8 October 2009

Communicated by: Associate Editor L. Vant-Hull

Abstract

The amount of energy contained in the solar aureole affects the performance of solar systems. Solar optical systems are, therefore, dependent on the characteristics of the shape of the sun in a specific geographical location. For this reason, the present study proposes the design of solid lenses and mirrors modelled from a set of concentric spherical rings that give a desired distribution of energy in the focal plane. One hundred spherical rings, whose optimum curvature radius values were calculated by Genetic Algorithms, were employed in the modelling process. The study also proposes a design of a petal tool to polish lens and mirror surfaces.

Keywords: Energy distribution; Genetic Algorithm; Solar concentrator; Spherical ring

1. Introduction

Optical design has two general aims: firstly, to obtain a high quality image with an optical system and secondly, to provide a sufficiently high concentration of energy flow to meet the geometric parameters of the system in terms of diameter, length, curvatures and thickness. Therefore, the space used by the system has to be taken into account. In accordance with this second aim, rings with spherical surfaces were used as optical elements to increase the diameter of the optical system and thereby maintain the resolution established by optical design in fluorescent detectors (Cordero-Dávila et al., 2000b), that is, its preestablished spherical aberration value. The Fluorescent Detector (FD) employed in the present case had two ring-shaped lenses. In each ring, the first surface is flat while the second is spherical. In the fabrication of these lenses, each ring was polished separately (Cordero-Dávila et al., 2000a). Spherical rings have been used to design a low-frequency Fresnel lens used as an FD (Diaz-Anzures and Cordero-Davila, 2000; Diaz-Anzures et al., 2004). In their design, the curvature radii of the rings were considered equal and were polished on the same mounting (Diaz-Anzures et al., 2004). Spherical rings have also been used to model adaptive liquid lenses with transparent elastic surfaces to simulate images generated by the lens (González-García et al., 2006a).

Lorenzo and Luque (1981) analysed a two-stage concentrator system whose first stage consists of a Fresnel lens

* Corresponding author. Address: Universidad Tecnológica de la Mixteca UTM, Km 2.5 Carretera a Acatlima, Huajuapan de León Oaxaca, C. P. 69000, Mexico. Tel./fax: +52 9535320399.
E-mail address: jgonzal@mixteco.utm.mx (J. González-García).

0038-092X/$ - see front matter © 2009 Elsevier Ltd. All rights reserved.
doi:10.1016/j.solener.2009.09.002

(either flat, roof shaped or curved). They demonstrated that the system that best generates the highest concentration of energy is one using a curved lens formed from an infinite number of segments (this generates a continuous surface), in such a way that the rays coming from the edges of the source and inciding on any point of the lens must reach the edges of the second-stage entry. Therefore the profile of the desired curved lens is such that the slope at each point must coincide with the angle corresponding to the locus which touches that point.

Drawing from the way the curved Fresnel lens works (Lorenzo and Luque (1981)), and research on spherical rings (Diaz-Anzures et al., 2004; González-García et al., 2006a), the present study proposes an alternative method for designing and fabricating lenses and mirrors that generate a desired energy distribution on a desired focal plane. These designs can be used as solar concentrators to create an optimised optical design for a specific geographical location (Buie et al., 2003). Such solid lenses or mirrors are designed under the assumption that their surfaces are formed from a set of 100 concentric spherical rings. The values of the curvature radii of each ring are different and optimum values are calculated with Genetic Algorithms (see Appendix A). Hence, this set of rings forms an aspherical surface. To facilitate the process of polishing the aspherical surfaces of these designs (using the classical method of fabricating optical surfaces) we propose the use of a petal tool to generate the desired surfaces.

2. Statement of the problem

This section describes the process of designing and polishing a lens formed from concentric spherical rings; this same process is applied in the case of a mirror formed from concentric spherical rings and is, therefore, omitted in this section.

2.1. Design of a Lens Formed from Concentric Spherical Rings (DLFCSR)

To simulate the DLFCSR (see Fig. 1(a) and (b)), an exact ray-tracing program for spherical surfaces (Smith, 1991) was developed in FORTRAN. The results produced by this program have already been reported for an adaptive

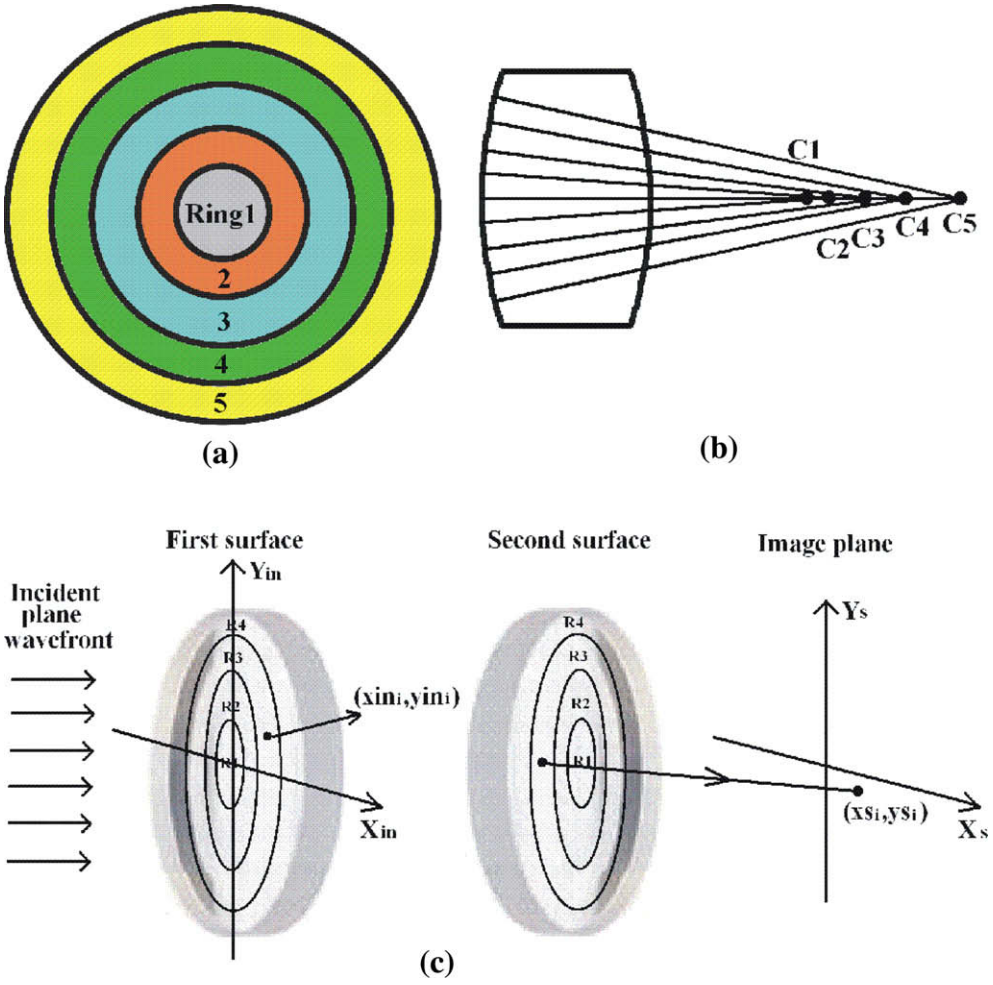

Fig. 1. Distribution of spherical rings on lens surfaces considered to be formed of five concentric spherical rings: (a) front view, (b) corresponding schematic diagram and (c) schematic diagram used to define the parameters used by genetic algoritms.

lens modelled by a set of spherical rings (González-García et al., 2006a).

One hundred rings were considered in the design of the lens, because the desired distribution of energy is obtained with this number. To generate the desired energy distribution with this lens, each ring had to have an established curvature radius value and therefore the number of variables to be optimised was 100. To reduce the number of variables to be optimised from 100 to 10, a recurrence formula (Chang and Lee, 1991; Cordero-Dávila et al., 2005; González-García et al., 2006b,c) was used to calculate the 100 curvature radius values. The recurrence equation for the 100 curvature radii is set as

$$r_{i+1} = r_i + \Delta r_j, \tag{1}$$

where r_i $(i = 1, \ldots, 100)$ are the curvature radii and Δr_j $(j = 1, \ldots, 10)$ are the curvature radius increments. These increments (González-García et al., 2006b) are the variables to be optimised by the Genetic Algorithm and are defined by the following equation

$$\Delta r_j = \begin{bmatrix} m_1 & \text{if} & 1 \leqslant i \leqslant 10 \\ m_2 & \text{if} & 11 \leqslant i \leqslant 20 \\ & \vdots & \\ m_{10} & \text{if} & 91 \leqslant i \leqslant 100 \end{bmatrix}. \tag{2}$$

Therefore, (xs_i, ys_i) coordinates of the Simulated Image (SI) on the image plane are a function of the increments defined by Eq. (2), so that

$$SI(r_{if}, r_{is}, xin_i, yin_i, m_1, m_2, \ldots, m_{10}) = (xs_i, ys_i), \tag{3}$$

where r_{if} and r_{is} are the curvature radius of each initial sphere of the polishing surfaces, (xin_i, yin_i) are the coordinates of the rays that intercept the first surface of the lens, see Fig. 1(c). Also, we assume that an incident plane wave front crosses the lens.

Once the coordinates of the Desired Image (DI) are determined,

$$DI(x_i, y_i) = (xd_i, yd_i), \tag{4}$$

and consequently, the sum of the squares of the errors between the points of the desired image and the simulated image is calculated, see Eq. (5)

$$S^2 = S_x^2 + S_y^2, \tag{5}$$

where $S_x^2 = \sum_{i=1}^{N} (xs_i - xd_i)^2$, $S_y^2 = \sum_{i=1}^{N} (ys_i - yd_i)^2$ and N is the number of points considered in the simulation. With Eq. (5), the rms function between the simulated and the desired image (or desired energy distribution) can be defined, see Eq. (6)

$$\text{Fitness function} = \text{rms} = \sqrt{\frac{S^2}{N-1}}. \tag{6}$$

Eq. (6) is what is used as a fitness function in applications of Genetic Algorithms to calculate the increments defined by Eq. (2). With these increments, Eq. (1) calculates the 100 curvature radii of the 100 rings that form the surface of the designed lens.

2.2. Design of the polishing tool: petal tool

One major obstacle is that aspherical optical surfaces are generally the most difficult surfaces to produce and are extremely expensive to fabricate (Small and Hoskins, 1986; Bajuk, 1976). To overcome the difficulty and expense of generating aspherical surfaces formed by the DLFCSR, we propose the use of petal tools that freely rotate (Cordero-Dávila et al., 2005). The experimental results from this type of tool have been quite acceptable.

In the design of the petal tool, we used the method of calculating the dwell-times of a set of complete annular tools acting on the surface of a workpiece using Genetic Algorithms (González-García et al., 2006b). To do so, the wear, h_{bi} $(i = 1, 2, \ldots, N_A)$ (known as base function) produced by each ring during a unitary time interval is calculated. Consequently, the desired wear h_D, as a function of the base functions, is expressed as

$$h_D = \sum_{i=1}^{M} \Delta t_i h_{bi}, \tag{7}$$

where t_i $(i = 1, 2, \ldots, N_A)$ are the dwell-times.

Dwell-times that generate desired wear are calculated and then converted by Eq. (8) to angular sizes α_i. From these, a petal tool is formed to generate the desired wear (Cordero-Dávila et al., 2005; González-García et al., 2006b,c). In Eq. (8), each dwell time t_i is divided by the maximum application time, T, and is multiplied by a 90° angle to form a 4-petal tool, as can be seen in the shaded area of Fig. 4(c)

$$\alpha_i = \left(\frac{t_i}{T}\right)(90^\circ) \tag{8}$$

3. Numerical results

This section presents the numerical results of two designs. In the first design, the desired energy distribution to be generated by DLFCSR corresponds to energy distribution on the optical axis by an achromatic doublet. In the second design, the mirror formed from concentric spherical rings is used to generate an angular size of the concentration of energy flow of approximately one order of magnitude smaller compared to the spot size generated with a spherical mirror.

3.1. First design: energy distribution generated by an achromatic doublet

Fig. 2 shows the distribution of energy generated by a classical achromatic doublet that is scaled by a factor of

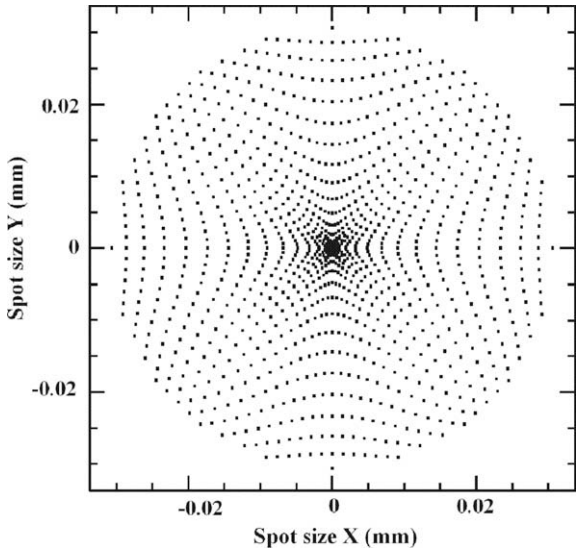

Fig. 2. Energy distribution generated by a classical achromatic doublet.

10 (because the original was very small and could not be reproduced by the DLFCSR). The distance at which the doublet generates this distribution is 391 mm from the back surface. The incoming light was defined as a parallel plane wave, i.e., light from a distant point source.

Three cases are considered for the DLFCSR. In each case, the distance of the energy concentration with respect to the second surface lens is different, the values of these distances being 380, 391.44 and 410 mm. The purpose of this is to show that it is possible to make a lens using DLFCSR for each position in order to generate this energy distribution. For these designs, the variables to be optimised are: (1) the curvature radius of each ring, (2) the curvature radius of each initial sphere of the polishing surfaces, (3) thickness and (4) refraction index, giving a total of 24 variables. Twenty of these variables are the radius increments with which we calculated the 200 curvature radii of the 200 spherical rings that make up the surfaces of the lens (100 for each surface).

The parameters of the Genetic Algorithm are described in Appendix A. The results obtained from the optimization are shown as follows: Fig. 3(a–c) show how the rms value between the distribution of desired and simulated energy decreases as generations go through the Genetic Algorithm; Fig. 3(d–f) show the corresponding distributions generated for image plane distances of 380, 391.44 and 410 mm, respectively.

Table 1 shows optimised values of curvature radius increments for the first and second surfaces of the DLFCSR for three positions of the energy concentration. Table 2 shows the corresponding curvature radii of the initial spheres for each surface and their respective axial thicknesses and refraction indexes. Table 3 shows energy distribution data of the energy generated with each DLFCSR.

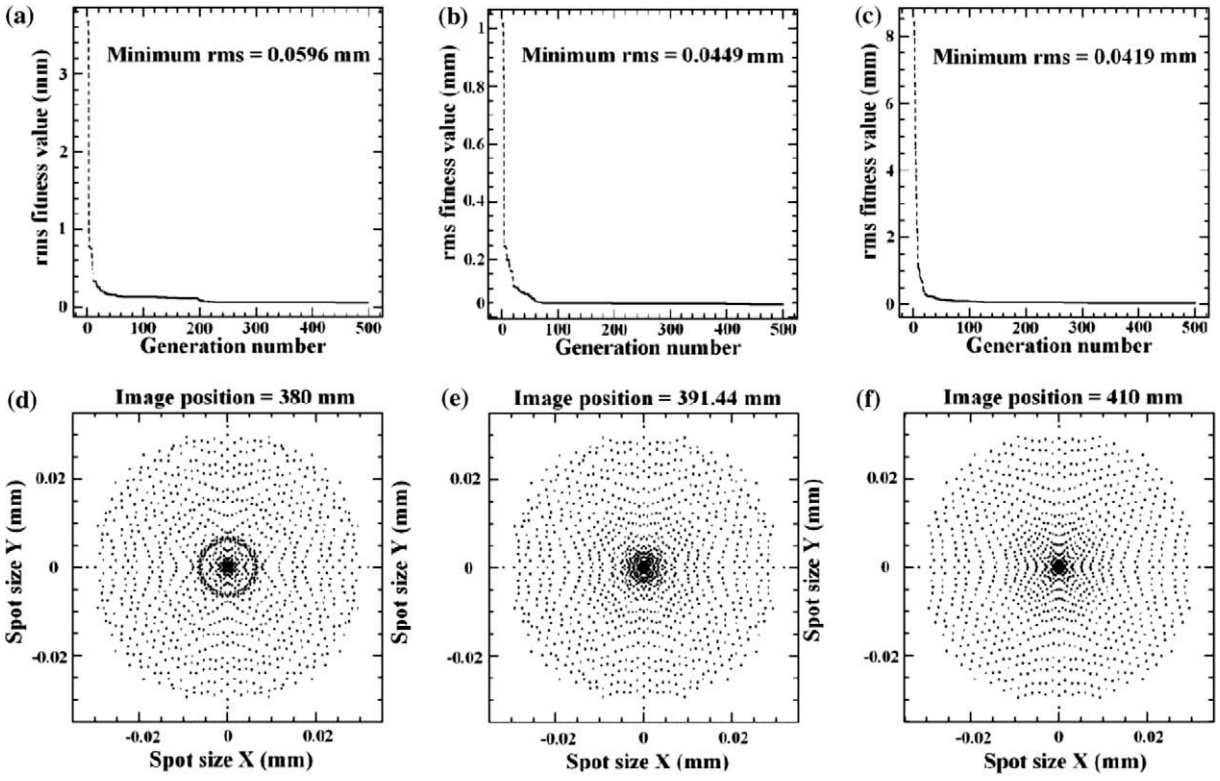

Fig. 3. Results of Genetic Algorithm optimization for the DLFCSR to generate a desired energy distribution formed by a classical achromatic doublet: (a–c) graphs of rms values against the number of generations, and the corresponding graphs of energy distribution generated for image plane positions (d) 380, (e) 391.44 and (f) 410 mm, respectively.

Table 1
Δr_j calculated using Genetic Algorithms for the first (F) and second (S) surface of the DLFCSR.

Δr_j	Value (mm) Position 1 380 nm F	Value (nm) Position 1 380 nm S	Value (nm) Position 2 391.44 nm F	Value (nm) Position 2 391.44 nm S	Value (nm) Position 3 410 nm F	Value (nm) Position 3 410 nm S
Δr_1	8.09132	6.04155	8.74202	8.02433	3.76639	5.17217
Δr_2	−1.38212	3.90923	−0.38822	2.51230	−0.89440	0.62185
Δr_3	1.39418	−2.85276	−1.28430	3.79814	0.35693	−4.86849
Δr_4	0.45841	2.10500	1.28018	−1.39601	2.54145	−4.95304
Δr_5	−0.50435	2.65819	1.90387	−0.72120	−0.23958	2.47995
Δr_6	2.50192	0.02395	2.96446	−4.07511	−0.04288	4.64356
Δr_7	−0.01480	4.84286	1.90006	1.60477	1.88388	−2.44912
Δr_8	2.18787	0.02823	3.00124	−1.11293	1.63666	0.08194
Δr_9	3.78791	−0.52342	4.38383	−1.19045	2.50131	0.19685
Δr_{10}	3.57717	3.36795	3.56816	3.41876	2.16528	4.95090

Table 2
Values calculated by GA of the curvature radii of initial spheres, axial thickness and the refraction index of each DLFCSR corresponding to each position.

Parameter	Position 1 380 mm	Position 2 391.44 mm	Position 3 410 mm
Curvature radius of the initial sphere for first surface (mm)	351.52468	329.36450	331.51641
Curvature radius of the initial sphere for second surface (mm)	588.41900	542.57241	757.38281
Thickness (mm)	42.92836	13.72855	16.48740
Refraction index	1.56367	1.51980	1.55567

Table 3
Distribution data of energy generated by each DLFCSR for three distinct positions.

Parameter	Classical achromatic doublet	DLFCSR Position 1	DLFCSR Position 2	DLFCSR Position 3
Image position (mm)	391.44	380	391.44	410
Total spot size (mm)	0.06121	0.06359	0.06369	0.06365
Geometrical spot size (mm)	0.01787	0.01788	0.01783	0.01789
Geometrical rms X/Y spot size (mm)	0.01264	0.01264	0.01261	0.01265
Angular spot size (°)	0.00896	0.00958	0.00931	0.00889

Results obtained on DLFCSR are intended to exemplify how, on the basis of the design of this lens, a desired energy distribution can be obtained, for example, of an achromatic doublet. The application which the DLFCSR would have in the field of solar energy would be in the formation of part of an optic system (once more as an example and as a possibility) to generate a desired irradiance distribution with a view to "reducing the effect of the solar aureole", in line with the established design aims (see Section 5).

3.2. Design of a mirror for concentrating energy flow

This case involves designing a mirror by means of concentric spherical rings to generate an angular size of the concentration of energy one order of magnitude smaller compared to the spot size generated with a spherical mirror. This design does not take into account the shape of the distribution of the resulting energy on the image plane of a parallel plane wave.

A spherical mirror with a 1500 mm diameter, a curvature radius of 4000 mm and a focal distance of 2000 mm (which are the parameters of a fluorescent detector (Diaz-Anzures et al., 2004)), generates a 0.20966° disc of least confusion at a distance of −1973.0 mm from the vertex of the mirror. Hence, the Mirror Designed with Concentric Spherical Rings (MDCSR) will be required to generate a concentration of energy of a desired angular size of 0.02096° at the same distance as that generated by the spherical mirror.

The Genetic Algorithm program for the MDCSR case will calculate 20 increments of curvature radii from which 100 curvature radii will be calculated of the 100 rings that form the mirror surface. The fitness function was established as the error square of the difference between the simulated angular size (sas) and the desired angular size (das):

$$\text{Fitness function} = S^2 = (\text{sas} - \text{das})^2 \tag{9}$$

Fig. 4(a) shows the graph of S^2 against the number of generations; Fig. 4(b) shows the graph of the optimised curvature radii of the rings against their radial position on the mirror surface. Table 4 shows the parameters of the MDCSR and the spherical mirror. The error (for an incoming plane wave) between the desired angular size and the size generated by MDCSR is approximately one hundredth of a degree.

Once the MDCSR is completed, the design of the petal tool polisher is initiated (Cordero-Dávila et al., 2005; González-García et al.,2006b,c). Hence, the diameter of the mirror to be polished and that of the petal tool are 1800 and 1500 mm, respectively, with an oscillation amplitude of 150 mm. The wear to be generated by a petal tool will begin

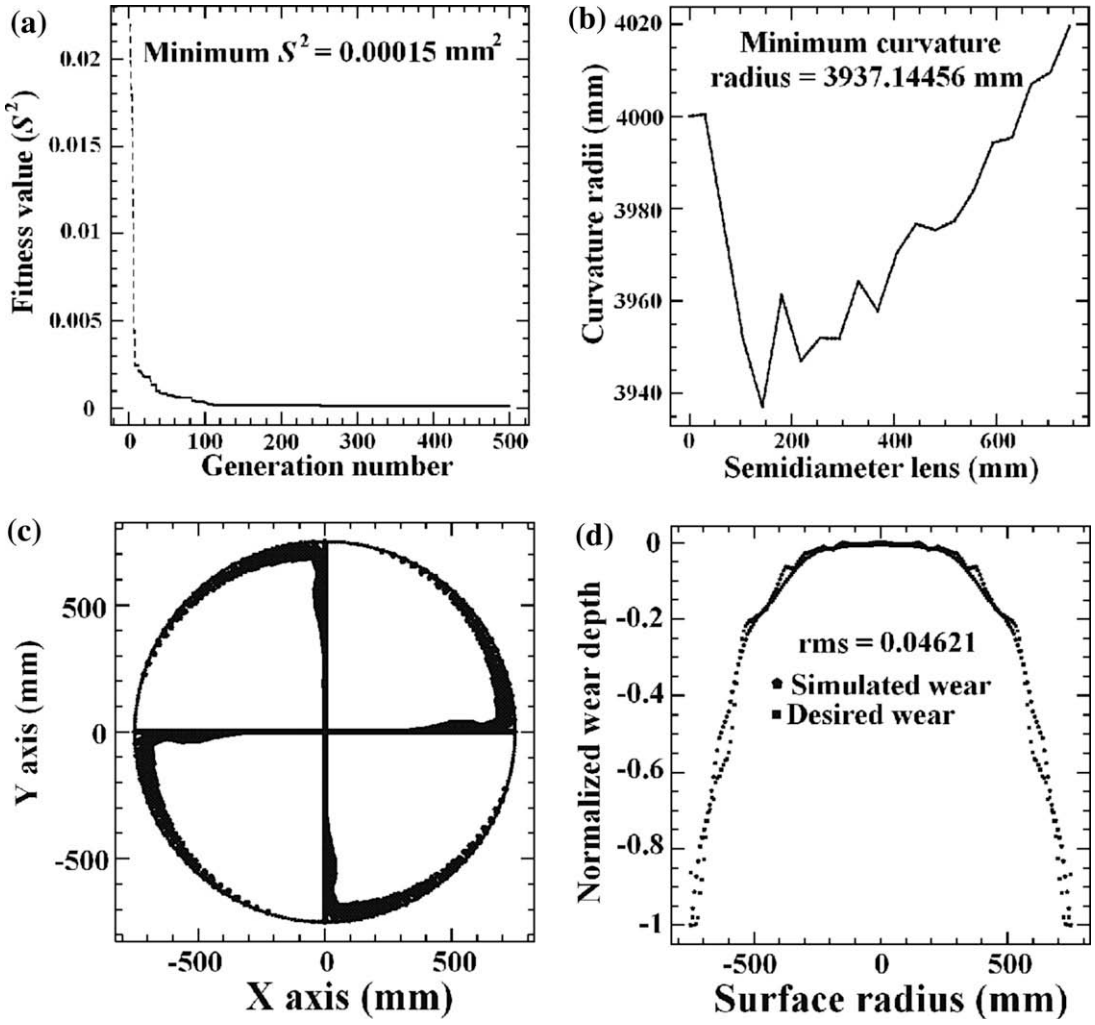

Fig. 4. Results obtained by the Genetic Algorithm program: (a) Plot of S^2 as a function of the number of generations, (b) plot of the curvature radii calculated, (c) petal tool designed and (d) plot of simulated wear generated by the tool and plot of desired wear.

Table 4
Energy distribution data generated by the spherical mirror and the MDCSR.

Parameter	Spherical mirror	MDCSR
Image position (mm)	−1973.0	−1973.0
Total spot size (mm)	7.21992	1.14793
Geometrical spot size (mm)	2.46796	0.32605
Geometrical rms X/Y spot size (mm)	1.74511	0.23055
Angular spot size (°)	0.20966	0.03333

on a sphere whose curvature radius value – 3937.14456 mm – is the least curvature radius value calculated by the Genetic Algorithm for the spherical rings that form the designed mirror, see Fig. 4(b). Fig 4(c) shows the petal tool designed with GA and the corresponding graph of generated wear is shown in Fig. 4(d).

In the Genetic Algorithm, the curvature radius value of the initial sphere (on which polishing began) was set at 4000 mm; this value is assigned to the central ring of the mirror, as can be seen in the graph in Fig. 4(b). One can also notice that in the case of a certain number of rings their corresponding curvature radii decrease. This is because the value of the curvature radius of the initial sphere is not the ideal one for initiating the wear, see Appendix B. Hence, in order to improve the results, a smaller curvature radius value can be proposed or this radius can become just another variable for the genetic algorithm.

In order to generate the desired wear shown in Fig. 4(d), the petal tool shown in Fig 4(c) (calculated with the Genetic Algorithm) was designed taking into account that this can rotate and oscillate in a simple harmonic movement (Cordero-Dávila et al., 2005).

4. Results obtained by considering the image of the sun as an object

This section presents the results obtained with the MDCSR (hereafter referred to as the 'mirror'). In order to develop the simulations, the sun was taken as an object in view of the fact that the distribution of sun irradiances is not constant; these simulations were carried out with the

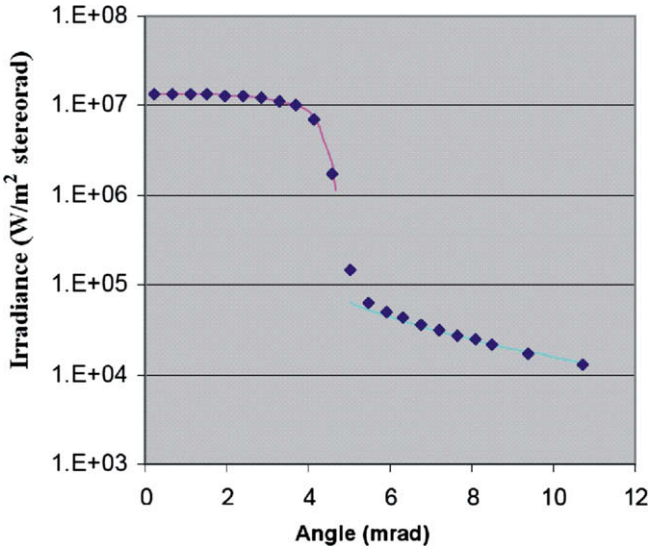

Fig. 5. Distributions of sun irradiances.

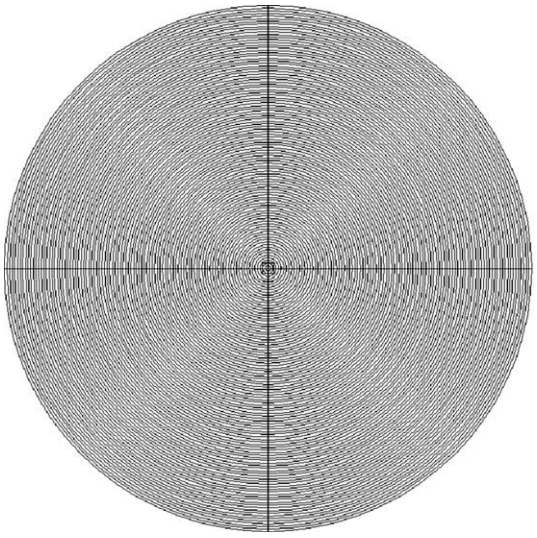

Fig. 7. Mirror simulated with the Zemax program.

Zemax version EE commercial optical design program (ZEMAX, Software For Optical System Design, 2008).

Experimental results show that irradiance distributions of the sun have two typical regions, as can be seen in Fig. 5. These are known as the solar disc and the aureole, respectively.

To generate the image of the sun to be used as an object for the mirror, the following equations were used:

The disc region was adjusted by this equation

$$B(\theta) = B_d\left[1 - (0.5051\theta/\alpha)^2 - (0.9499\theta/\alpha)^8\right], \quad (10)$$

where $B_d = 13.639 \times 10^6$ W/m^2 stereorad and $\alpha = 4.653$ rad, while the aureole region was adjusted by this equation

$$B(\theta) = B_\alpha(\theta/\alpha)^{-2}, \quad (11)$$

where $B_\alpha = 72{,}200$ W/m^2 stereorad.

The sun image before entering the mirror (at a distance of 150 mm from its vertex) is shown in Fig. 6. In this case, the detector used by Zemax was programmed with a 1600 mm detecting diameter, 100 mm bigger than the diameter of the mirror, in order to ensure complete detection of the irradiance of the sun. The image of the mirror simulated with the Zemax program is shown in Fig. 7.

Figs. 8–10 show results obtained with Zemax of images generated by a parabolic mirror, a spherical mirror, and the MDCSR, respectively, at a distance of 2000 mm from their vertices. With a view to showing a quantitative comparison of the results, the FWHM (Full Width at Half Maximum) criterion was used to quantify the size of the images generated by these mirrors. The FWHM is an easy way to define the width of a beam. This criterion is an expression of the extent of a function, given by the difference between the two extreme values of the independent variable at which the dependent variable is equal to half of its maximum. Table 5 shows the results of sun image sizes using the above-mentioned criterion.

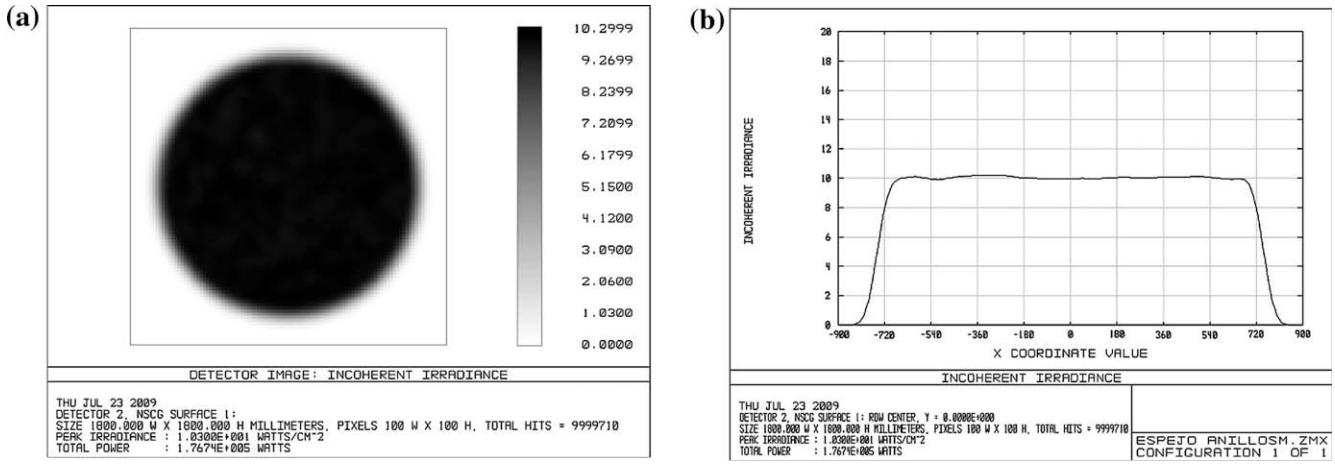

Fig. 6. Flux distribution of the sun simulated with the Zemax program: (a) front view; (b) cross-section.

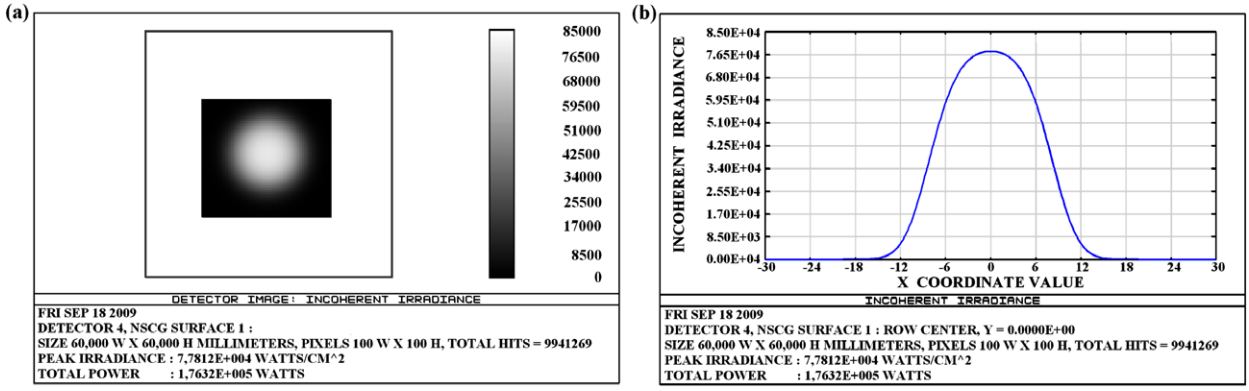

Fig. 8. Sun image generated with a parabolic mirror: (a) spot diagram and (b) graph of irradiance distribution.

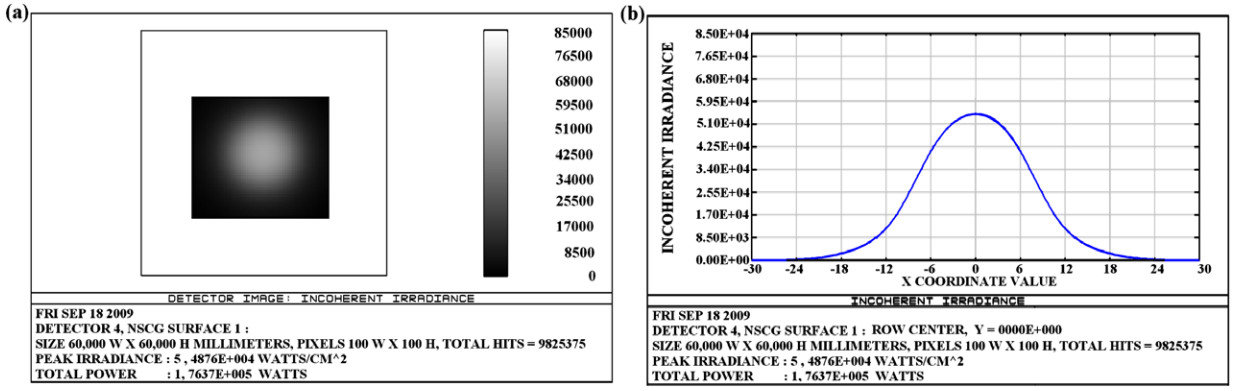

Fig. 9. Sun image generated with a spherical mirror: (a) spot diagram and (b) graph of irradiance distribution.

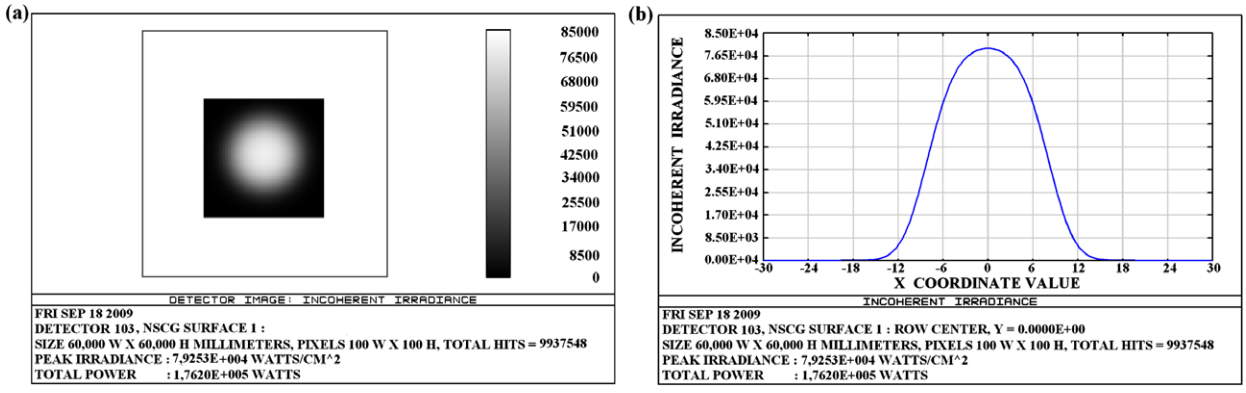

Fig. 10. Sun image generated with the MDCSR: (a) spot diagram and (b) graph of irradiance distribution.

Results in Table 5 show that the size of the image generated by the MDCSR is between the sizes generated by parabolic and spherical mirrors (closer to the one generated by the parabolic mirror). These results show that it is possible to design mirrors from the concept of a set of concentric spherical rings to generate a desired concentration of energy. Obviously, one order of magnitude smaller compared to the spherical mirror was not obtained with the MDCSR (as it was designed for a point object, that is, a parallel plane wave). This is because the image of the sun has an angular size of half a degree, in other words, it is not a point source. Such is the situation that the difference between the size of images in the MDCSR and the parabolic mirror (which is the mirror that generates the sun image size predicted by the theory, see Appendix C) is approximately 1.4 mm (see Table 5). Hence, the advantage in using an MDCSR is that by optimizing the curvature radii of spherical rings that generate the surface of the

Table 5
Results of image sizes generated by different types of mirrors using the FWHM criterion.

Mirror type	Size of sun image (mm)
Parabolic	15.41
Spherical	18.58
MDCSR	16.82

MDCSR it is possible to control the shape of the sun image, or its distribution of irradiance, in for example, a specific field of vision. This would not be possible with a parabolic mirror because of coma aberration.

5. Application

Buie and Monger (2004) analyzed the influence of the amount of circumsolar radiation in function of the acceptance angle of the absorber. They show the relationship between the optical efficiency (percentage of total energy) and size of the absorber in a specific line focus Fresnel concentrator to various CSRs. Sunshapes with CSR between 0.02 and 0.2 were modelled, see Fig. 11. The CSR is defined as the radiant flux contained within the circumsolar region of the sky divided by the incident radian flux from the direct beam and aureole. These results showed that as the CSR of the sunshape increase, the size of the absorber must also increase to accommodate a similar amount of energy, that is, the size of the image increases and therefore the design of mirrors and lenses from a set of concentric spherical rings can be used in the field of solar energy to generate optic systems which enable us to obtain the maximum possible concentration of energy. This means reducing the effect of the solar aureole by taking as a fitness function the angular size of the sun image or its corresponding desired graph of irradiance distributions for a specific location (determined CSR value (Buie and Monger (2004)), thereby optimizing the angular size of the absorber.

6. Conclusions

This study presented the theoretical procedure used to design and manufacture lenses that form a desired distribution of energy, and mirrors that generate a desired angular size of the concentration of energy. Within the design, surfaces were considered to be formed from a set of concentric spherical rings and the optimum curvature radius values of each ring were calculated with Genetic Algorithms. For the fabrication of these designs, a petal tool for polishing surfaces was proposed. This polishing tool was calculated using Genetic Algorithms.

The advantages of the design and fabrication of these types of lenses and mirrors by means of a set of spherical surface rings are: (1) the creation of designs that generate a distribution of energy that is the nearest possible to the desired distribution of energy generated by optical systems such as doublets, (2), the creation of mirror designs that reduce the angular size of the energy captured. The size of mirrors can thereby be increased (to capture greater amounts of energy) and the angular size of the energy can be maintained, or even reduced, in specifically desired positions, (3) the aspherical surfaces of the proposed lenses and mirrors are more easily polished since it only uses a petal tool that is specifically designed to generate desired wear. Polishing begins on an initial sphere whose optimum

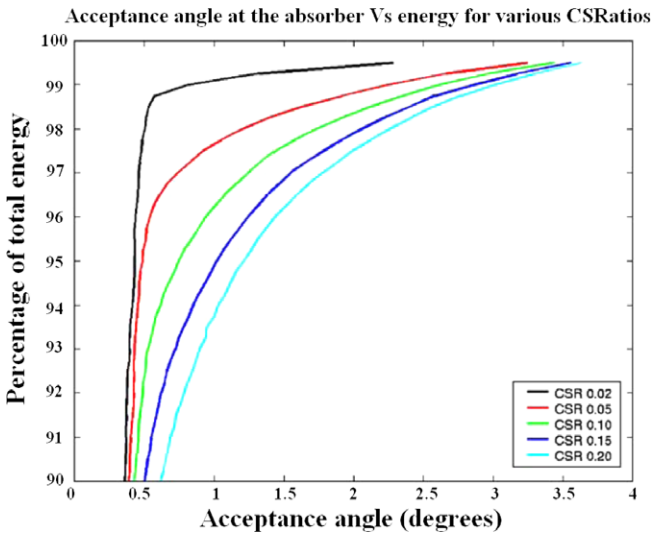

Fig. 11. The overall optical efficiency of a line focus imaging concentrator plotted against the acceptance angle of the absorber for various circumsolar ratios. This figure was obtained from the following reference: Buie and Monger (2004).

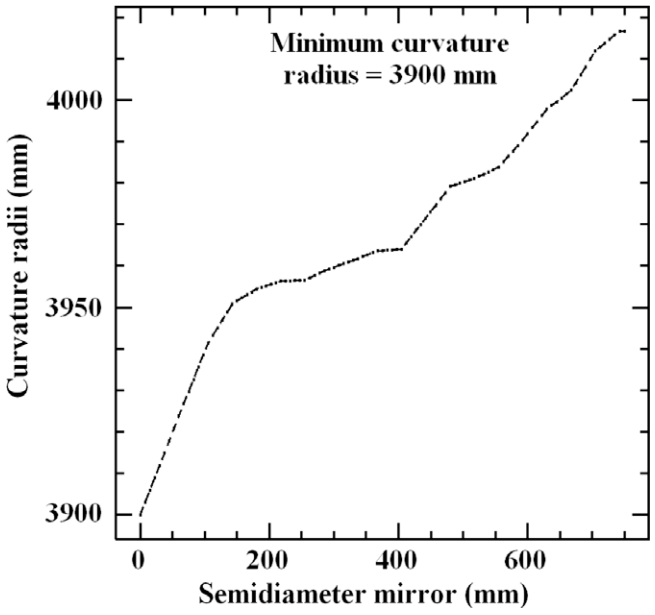

Fig. 12. Graph of the optimised curvature radii of the rings against their radial position on the mirror surface.

curvature radius value can be the minimum value of the optimum curvature radii calculated from the spherical rings that will form the surface. Polishing time can thereby be saved because spheres are relatively easy to generate. Furthermore, petal tool polishing is more efficient than that of a small solid tool because the diameter of a petal tool is practically the same as that of the workpiece to be polished. The whole workpiece area can thereby be polished at the same time.

Acknowledgments

The authors thank CONACYT for supporting this research project entitled "Óptica Adaptiva de Sistemas Refractores" (Adaptive Optics of Refractor Systems Project) registered under No. SEP-2004-C01-46080. Our thanks also to Patrick Rafferty (KFUPM University, Saudi Arabia. rpatrick@kfupm.edu.sa) for translating the original document from Spanish to English.

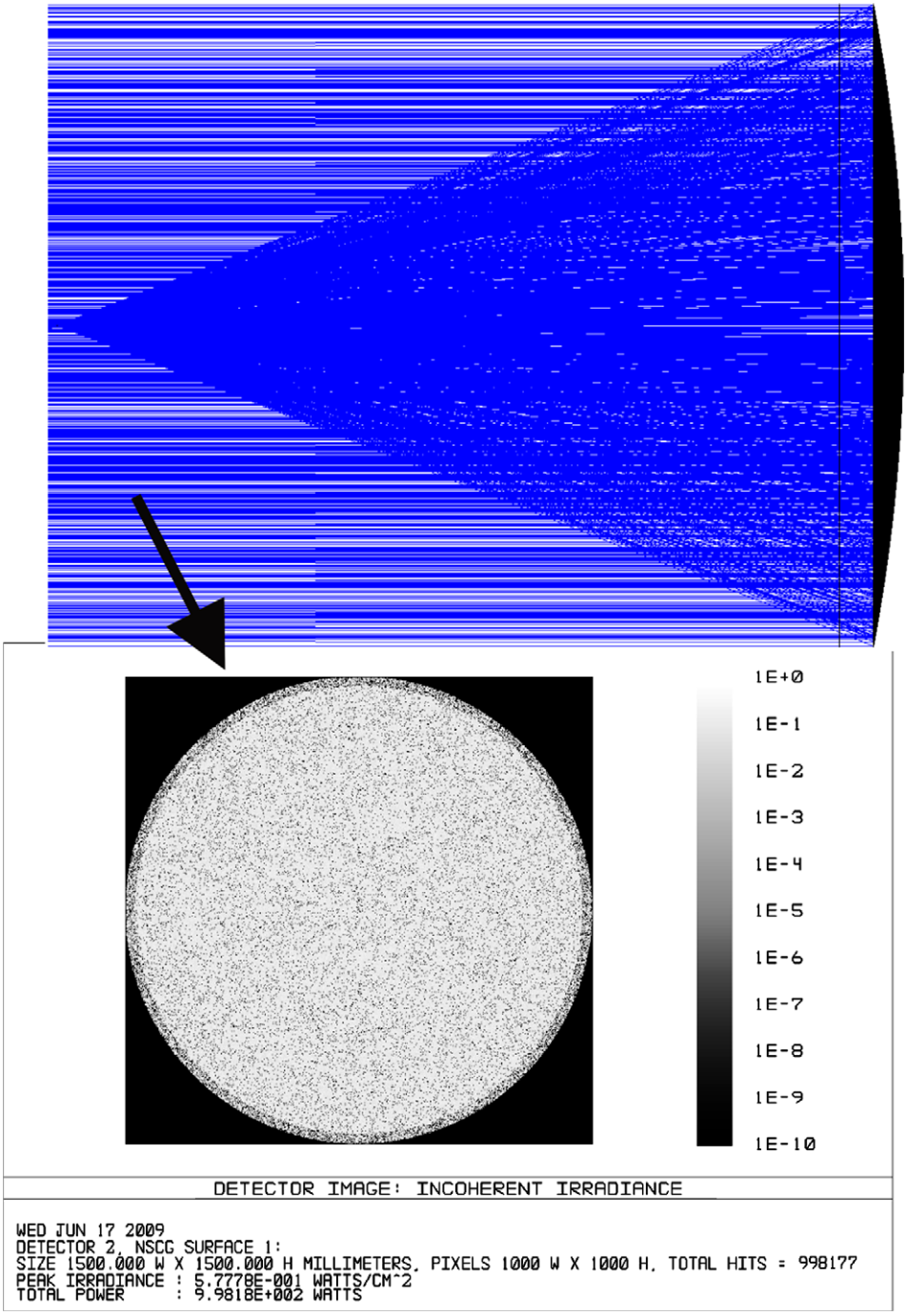

Fig. 13. Plane wave front with its corresponding energy distribution.

Appendix A. Parameters of the Genetic Algorithm

The Genetic Algorithm program used a population size of 160 members, doing a search over 500 generations. The selection process employed the *tournament* technique (Millar and Goldberg, 1995), which consists of randomly taking a certain number of individuals from the population, called *tournament size*; from this, one of the individuals of the set is chosen for the next generation. The process is repeated as many times as there are individuals in the population, in the present case 160 times. This technique uses a probability value, called *selection probability*, which is calculated as the inverse of the size of the tournament even though this probability could, in fact, be greater. The size of the tournament implemented in the present study was two (typical value), with a selection probability of 0.95. Better results were found with this value than with 0.5 (inverse of two) (Cordero-Dávila et al., 2007). In order to determine which individual gets chosen from among the two randomly selected candidates of the population, both are evaluated by the fitness function to identify the better of the two. Later, a random number between 0 and 1 is generated and if this is less than the selection probability value, the better of the two individuals is selected. Otherwise, the other individual is selected. Both individuals are then returned to the initial population in order to continue once more with the selection of individuals. The crossover technique define was implemented at a point with a crossover probability of 0.7. The mutation technique defined was one in which all the genes of each chromosome of the population had the same proba-

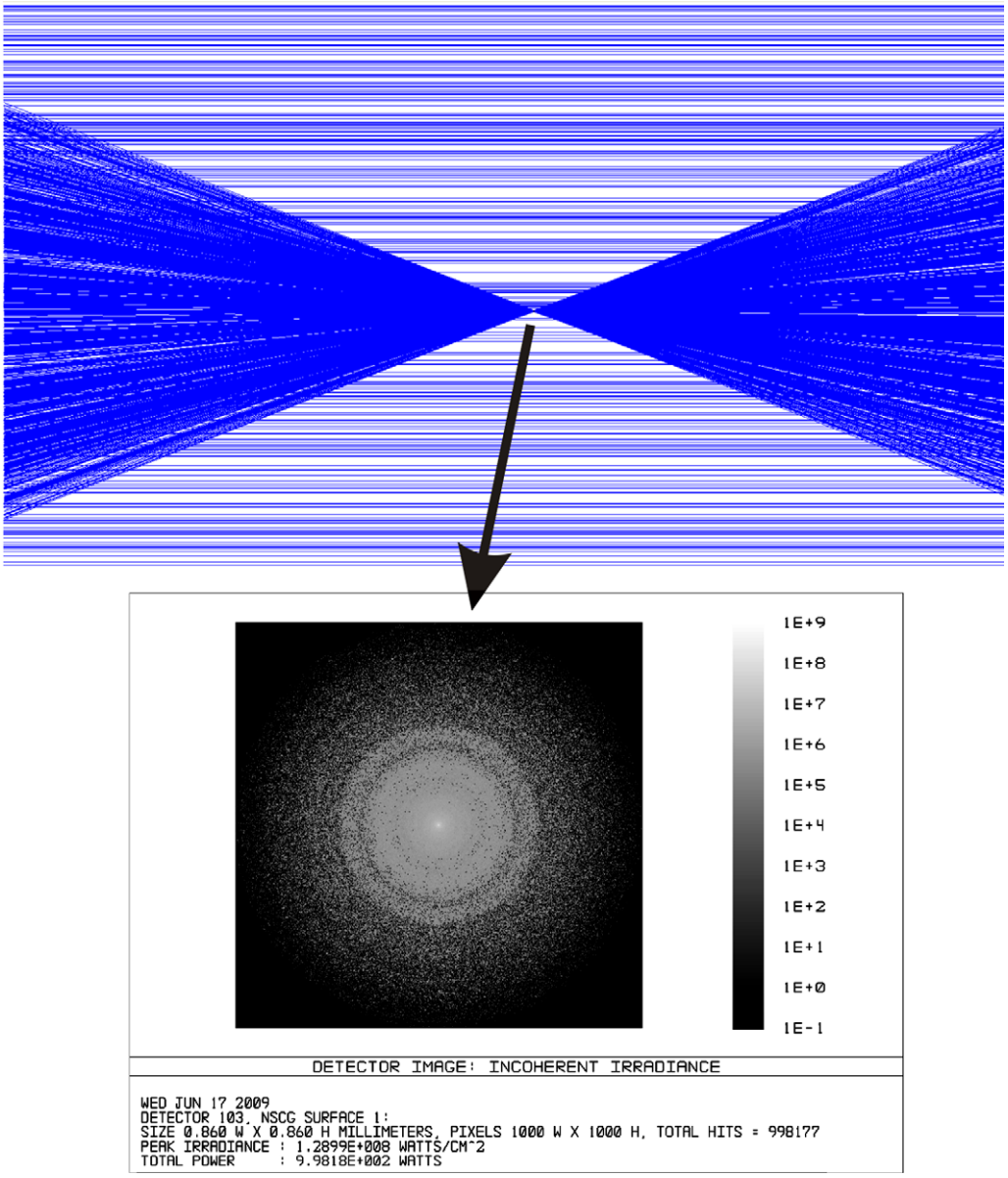

Fig. 14. Concentration of rays of the disc of least confusion with its corresponding energy distribution.

bility of being mutated. The mutation probability value was the inverse of the size of the population (González-García et al., 2006a; Goldberg, 1992).

Appendix B. MDCSR simulations for a point source considering an initial radius of 3900 mm using Zemax

In Section 3, an initial radius of 4000 mm was considered for the MDCSR (a curvature radius of the initial sphere to be polished). This design generated curvature radii that were shorter than the initial radius, as shown in Fig. 4(b). To avoid this abrupt reduction of the curvature radii, a new design was made in which the initial curvature radius was now considered to have a value of 3900 mm. The optimal curvature radius values found with the Genetic Algorithm (by means of Δr) are shown in the graph in Fig. 12 where the radii tend to get bigger and smoother. Fig. 13 shows the plane wave front and its corresponding distribution of energy simulated with Zemax, before arriving at MDCSR. Fig. 14 shows the concentration of rays after reflection together with the distribution of irradiance of the circle of least confusion. The size of the angular image obtained with the simulation done with Zemax (Fig. 14) was 0.0225°. This value is practically in agreement with the MDCSR design to generate a concentration of energy to a size of one order of magnitude smaller than that of the spherical mirror.

Appendix C. Theoretical size of the sun image

The angular size of the image of the sun generated by the mirror that the theory predict is given by

$$h = f\theta, \tag{12}$$

where θ is the angular size of the sun and f is the focal length of the mirror, considering that the mirror has a focal length of 2000 mm and an angular size of the sun of 8.7×10^{-3} rad, the theory predicts an image size of the sun of 17.45 mm.

References

Bajuk, D.J., 1976. Computer controlled generation of rotationally symmetric aspheric surfaces. Opt. Eng. 15, 401–406.

Buie, D., Monger, A.G., Dey, C.J., 2003. Sunshape distributions for terrestrial solar simulations. Sol. Energy 74, 113–122.

Buie, D., Monger, A.G., 2004. The effect of circumsolar radiation on a solar concentrating system. Sol. Energy 76, 181–185.

Chang, R.-S., Lee, P.-Y., 1991. Computer simulation of loose abrasive grinding aspherical optical surface by local figuring pitch. In: Doherty, V.J. (Ed.), Proceedings of Advanced Optical Manufacturing and Testing II. Proc. SPIE, 1531, pp. 312–317.

Cordero-Dávila, A., Cabrera-Peláez, V., Cuautle-Cortés, J., González-García, J., Robledo-Sánchez, C., Bautista-Elivar, N., 2005. Experimental results and wear predictions of petal tools that freely rotate. Appl. Opt. 44, 1434–1441.

Cordero-Dávila, A., González-García, J., Cuautle-Cortes, J., Robledo-Sáchez, C., Cabrera-Pelaéz, V., 2000a. Segmented Spherical Corrector Rings 2: Experimental Results. In: Salazar, U., Villaseñor L., Zepeda, A. (Eds.), Proceedings of Observing Ultrahigh Energy Cosmic Rays From Space And Earth, vol. 566. AIP Conference Proceedings, pp. 357–360.

Cordero-Dávila, A., Robledo-Sáchez, C., González-García, J., Cabrera-Pelaéz, V., 2000b. Segmented Spherical Corrector Rings 1: Computer simulations. In: Salazar, U., Villaseñor, L., Zepeda, A. (Eds.), Proceedings of Observing Ultrahigh Energy Cosmic Rays From Space And Earth, vol. 566. AIP Conference Proceedings, pp. 354–356.

Cordero-Dávila, A., Téllez-Arriaga, L., González-García, J., Robledo-Sánchez, C.I., Cuautle-Cortés, J., Díaz-Anzures, J.J., Martinez-Medina, L.A., 2007. Calculating subtool pressure by using genetic algorihms. In: Yang, L., Chen, Y., Kley, E.B., Li, R. (Eds.), . In: Proceedings of 3rd International Symposium on Advanced Optical Manufacturing and Testing Technologies: Advanced Optical Manufacturing Technologies, vol. 6722. Proc. SPIE, p. 672204.

Diaz-Anzures, J., Cordero-Davila, A., 2000. Fresnel mirrors for fluorescence detectors. In: Salazar, U., Villaseñor L., Zepeda, A. (Eds.), Proceedings of Observing Ultrahigh Energy Cosmic Rays From Space And Earth, vol. 566. AIP Conference Proceedings, pp. 385–388.

Diaz-Anzures, J., Cordero-Dávila, A., González-García, J., Martinez-Bravo, O., Robledo-Sanchez, C., Khrenov, B.A., Garipov, G.K., 2004. Low frequency Fresnel mirrors for fluorescence detector telescopes. Astroparticle Phys. 21, 407–413.

Goldberg, D.E., 1992. Genetic Algorithms in Search, Optimization, and Machine Learning. Addison Wesley.

González-García, J., Santiago-Alvarado, A., Vázquez-Montiel, S., Cordero-Dávila, A., Castro-González, G., Vera-Díaz, E., López-López, A., 2006a. Exact ray tracing for an adaptive liquid lens with elastic surfaces. In: Mouroulis, P.Z., Smith, W.J., Johnson, R.B. (Eds.), . In: Proceedings of Current Developments in Lens Design and Optical Engineering VII, vol. 6288. Proc. SPIE, 62880T.

González-García, J., Cordero-Dávila, A., Leal-Cabrera, I., Robledo-Sánchez, C.I., Santiago-Alvarado, A., 2006b. Calculating petal tools using genetic algorithms. Appl. Opt. 45, 6126–6136.

González-García, J., Cordero-Dávila, A., Leal-Cabrera, I., Robledo-Sánchez, C.I., Castro-González, G., Santiago-Alvarado, A., Manzano-Sumano, L.J., 2006c. Design of petal tools based on the dwell-times of annular tools to generate convex surfaces. In: Program of the 49th Congreso Nacional de Física de la Sociedad Mexicana de Física, Bull. Soc. Mex. Suppl. vol. 20. pp. 126.

Lorenzo, E., Luque, A., 1981. Fresnel lens analysis for solar energy applications. Appl. Opt. 20, 2941–2945.

Millar, B.L., Goldberg, D.E., 1995. Genetic algorithms tournament selection, and the effects of noise. Complex Syst. 9, 193–212.

Small, D.W., Hoskins, S.J., 1986. An automated aspheric polishing machine. In: Sanger, G.M. (Ed.), . In: Proceedings of Optical Manufacturing, Testing and Aspheric Optics, vol. 645. Proc. SPIE, pp. 66–74.

Smith, W.J., 1991. Modern Optical Engineering, second ed. McGraw-Hill, Inc..

ZEMAX, Software For Optical System Design, 2008. Available from: <www.zemax.com>.